CrossMark
← click for updates

Nano- and micro-patterning biotemplated magnetic CoPt arrays†‡

J. M. Galloway,*[a,b] S. M. Bird,[c] J. E. Talbot,[d] P. M. Shepley,[a] R. C. Bradley,[e] O. El-Zubir,[c,f] D. A. Allwood,[e] G. J. Leggett,[c] J. J. Miles,[d] S. S. Staniland[c] and K. Critchley[a]

Patterned thin-films of magnetic nanoparticles (MNPs) can be used to make: surfaces for manipulating and sorting cells, sensors, 2D spin-ices and high-density data storage devices. Conventional manufacture of patterned magnetic thin-films is not environmentally friendly because it uses high temperatures (hundreds of degrees Celsius) and high vacuum, which requires expensive specialised equipment. To tackle these issues, we have taken inspiration from nature to create environmentally friendly patterns of ferromagnetic CoPt using a biotemplating peptide under mild conditions and simple apparatus. Nano-patterning *via* interference lithography (IL) and micro-patterning using micro-contact printing (µCP) were used to create a peptide resistant mask onto a gold surface under ambient conditions. We redesigned a biotemplating peptide (CGSGKTHEIHSPLLHK) to self-assemble onto gold surfaces, and mineralised the patterns with CoPt at 18 °C in water. Ferromagnetic CoPt is biotemplated by the immobilised peptides, and the patterned MNPs maintain stable magnetic domains. This bioinspired study offers an ecological route towards developing biotemplated magnetic thin-films for use in applications such as sensing, cell manipulation and data storage.

Introduction

Micro- and nano-patterned thin-films of magnetic materials are used in a wide range of devices. Patterns of low coercivity 'soft' magnetic thin-films are used for sorting and manipulating cells and magnetic beads,[1,2] in sensors,[3,4] and in studying 2D spin-ices;[5,6] whilst high coercivity 'hard' magnetic thin-films are used in data storage media.[7] CoPt is magnetically soft in its disordered A1 phase, but L1$_0$ ordered CoPt is magnetically hard and can form films with extremely high out-of-

[a]*School of Physics and Astronomy, University of Leeds, Woodhouse Lane, Leeds, LS2 9JT, UK*

[b]*School of Chemistry, University of Bristol, Cantock's Close, Bristol, BS8 1TS, UK. E-mail: johanna.galloway@bristol.ac.uk*

[c]*Department of Chemistry, University of Sheffield, Dainton Building, Brook Hill, S3 7HF, UK*

[d]*School of Computer Science, University of Manchester, Kilburn Building, Oxford Road, Manchester, M13 9PL, UK*

[e]*Department of Materials Science and Engineering, University of Sheffield, Sir Robert Hadfield Building, Maplin Street, Sheffield, S1 3JD, UK*

[f]*School of Chemistry, University of Newcastle, Chemical Nanoscience Laboratories, Bedson Building, Newcastle Upon Tyne, NE1 7RU, UK*

†The data presented in this article are openly available from the University of Leeds data repository http://doi.org/10.5518/43

‡Electronic supplementary information (ESI) available: Extended experimental details, extended discussion, and; supplementary diagrams, SEM images, EDX, XRD, SAED, VSM, MOKE, and MFM. See DOI: 10.1039/c6nr03330j

plane magnetic anisotropy[8–10] in grains with a diameter above ≈5 nm.[11] Therefore, these alloys are ideal candidates for use in a range of applications, with the L1$_0$ phase particularly suited for use in high-density data recording.[8–10] Nano-patterning of magnetic thin-films can be used to create bit-patterned media (BPM),[12] which offers an ultra high-density data storage solution. Conventional synthesis of patterned thin-films of magnetic nanoparticles (MNPs) requires high temperatures (≈500 °C), high vacuum sputtering and advanced patterning equipment.[8–10] These techniques are energy and resource intensive, and therefore expensive. As such, we have taken inspiration from nature to develop alterative fabrication routes that do not require such high cost, energy intensive manufacturing processes to create micro- and nano-patterned magnetic thin-films.

Biomineralisation proteins control the crystallisation and assembly of a range of minerals using mild, aqueous chemistry.[13–16] These include calcium carbonate shells,[17] hydroxyapatite teeth,[18] silica sponges and diatoms,[19,20] and magnetite in magnetotactic bacteria.[21–23] These biominerals often have improved properties[24] such as; tough calcite shells,[25] light guiding silica,[26] or an enhanced magnetic moment in magnetite.[27] Magnetite can be biotemplated onto a surface,[28,29] and can be patterned on surfaces,[30–33] but its coercivity is low. The coercivity of biotemplated magnetite can be increased by the addition of cobalt,[34,35] but this increase is still too small for high-density data storage applications.

Furthermore, these particles are too large for use in sensing or other magnetic thin-film applications. Fortunately, technologically relevant materials can be biotemplated by peptides,[15,16,36–40] and include: platinum,[41] $L1_0$ platinum alloys,[36,38,42,43] gold,[44,45] silver,[46] and semi-conductor quantum dots.[38,47]

We have recently shown that a biotemplating peptide is able to control the formation of $L1_0$ CoPt MNPs onto a silicon substrate,[43] but it was not possible to pattern this system well.[48] We previously reported the patterning of biotemplated magnetite[30–33] and cobalt doped magnetite[35] on Au surfaces using interference lithography (IL)[32,49] and micro-contact printing (µCP)[50–52] Fig. 1). We used self-assembled monolayers (SAMs) of an oligoethylene glycol functionalised alkanethiol to define polyethylene glycol (PEG) regions that resist the binding of proteins and peptides. In this paper, we have adapted these methods to pattern biotemplated CoPt for the first time. We have engineered a $L1_0$ CoPt biotemplating peptide sequence[42] for attachment to a gold surface. Cysteine (C) was added to a flexible linker (GSG) at the N-terminus of the CoPt biotemplating peptide (KTHEIHSPLLHK) to create a cysteine tagged CoPt biotemplating peptide (cys_CoPt, C-GSG-KTHEIHSPLLHK). The cys_CoPt peptide binds to the bare gold areas on the IL and µCP patterned surfaces *via* the sulfur in cysteine. This creates areas that selectively resist or promote the biomineralisation of CoPt in defined patterns on a surface (Fig. 1). Our

patterning strategy offers excellent control over the positioning of a layer of tightly packed monodispersed MNPs, and offers promise for developing this as an environmentally friendly route to produce biotemplated magnetic thin-films. Such patterned magnetic thin-films can be used for sensing or cell sorting (low coercivity), or in high-density data storage in BPM (high coercivity).

Results and discussion

Nanoparticle patterns are biotemplated under mild conditions

Nano-patterning using interference lithography (IL). We used IL[49] to form nano-patterns of biotemplated CoPt MNPs for the first time. We first formed homogenous PEG SAMs, and exposed them in the interferometer. In the regions where the SAM was exposed to a maximum in the interferogram, the adsorbed alkanethiols were removed to reveal bare gold regions at ambient conditions, as detailed by Bird *et al.*[32] We backfilled the bare gold nano-lines with the cys_CoPt peptide before biomineralisation with CoPt. Fig. 2a–c shows the biomineralised nano-lines that extend over the sample surface (≈1 cm²). The scanning electron microscopy (SEM) images show excellent contrast between the areas functionalised with the PEG (average width of a line (AW) is 109 ± 13 nm) and the areas biomineralised by the cys_CoPt peptide. The PEG SAM areas are free of particles, whereas the areas functionalised with cys_CoPt (AW is 226 ± 20 nm) are covered in a densely packed thin-film of MNPs. This demonstrates that the cys_CoPt peptide is capable of patterning biotemplated MNPs on the nano-scale, which is ideal for the development of bio-templated nano-sensors or BPM.

Micro-patterning using micro-contact printing (µCP). Fig. 2d–f, S2 & S3‡ show micro-patterned lines and squares of biotemplated nanoparticles formed using µCP SAMs. The biotemplated areas have a high density of nanoparticles formed onto the surface (Fig. 2f). The µCP line width is consistent across the patterned surface, with the PEG (AW is 6.1 ± 0.4 µm) separating the biotemplated MNPs (AW is 8.1 ± 0.3 µm). There are some larger composite particles on top of this biotemplated area, but the majority of the material is a uniform monolayer of biotemplated particles. Such micro-scale patterns of magnetic thin-films are of an ideal size for use in cell sorting and manipulation. This SAM-cys_CoPt peptide system on gold has significantly improved contrast when compared to patterning biotemplated MNPs on silicon.[48] The CoPt surface biomineralisation system presented here is highly adaptable. The ability to consistently pattern a thin-film of the bio-templated MNPs across the micro- and nano-scales offers scope for their development for use in a wide range of magnetic sensing, sorting and recording applications.

Optimising mineralisation of CoPt on patterned surfaces. We previously reported that a molar excess of Co^{2+} to Pt^{2+} (3 : 1) in the mineralisation solution is necessary to achieve the desired 1 : 1 ratio of Co : Pt in the biotemplated metallic MNPs.[43,48] Here we find that control of the metallisation temp-
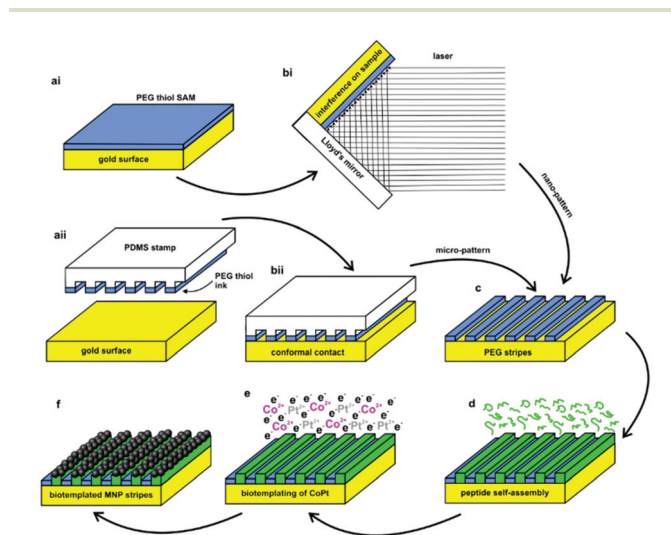

Fig. 1 Schematic of nano- and micro-patterning biotemplated CoPt MNPs onto surfaces. (ai) A self-assembled monolayer (SAM) is formed from an ethanol solution onto a gold surface and (bi) nano-patterned using interference lithography (IL)[49] (Fig. S1‡). (aii) Micro-patterns are formed using a PDMS stamp inked with a PEG thiol and (bii) brought into contact with a clean gold surface using micro-contact printing (µCP). (c) The PEG alkanethiol forms stripes that resist biomolecule binding. (d) The patterned surface is then immersed in a solution of the cys_CoPt peptide. The sulfur in the cysteine binds the peptide to the exposed areas of the patterned gold surface. (e) The biotemplating surface is immersed in an aqueous solution containing cobalt and platinum salts, and a reducing agent is injected at 18 °C under an N₂ atmosphere. (f) The salts are reduced to form MNPs, which are biotemplated onto the peptide immobilised onto the surface to form patterns of CoPt MNPs.
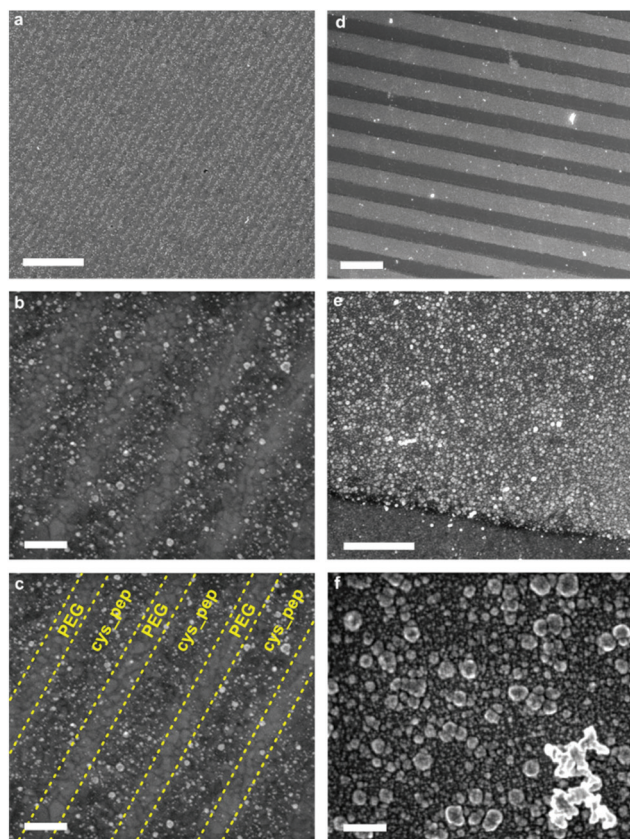
Fig. 2 Scanning electron microscope (SEM) images of biotemplated CoPt nano- and micro-patterned line surface. (a) Zoomed out and (b) zoomed in SEM image of biotemplated nano-lines. (c) Annotated version of image (b) to show areas functionalised with biotemplating peptide (cys_CoPt, average width (AW) is 226 ± 20 nm), which are mineralised with a closely packed layer of MNPs, and areas functionalised to resist mineralisation (PEG, AW is 109 ± 13 nm). (d) Micro-patterned lines of dark contrast are the gold surface that was protected against biomineralisation by the μCP PEG thiol (AW is 6.1 ± 0.4 μm). Lines of light contrast were backfilled with the cys_CoPt peptide before metallisation with CoPt, and are covered in a biotemplated layer of MNPs (AW is 8.1 ± 0.3 μm). (e) A closer view of an edge of a patterned line showing the clean, unbiomineralised gold (bottom of image) and the surface biotemplated MNPs (top of image). (f) A closer view of the biotemplated MNPs, showing a consistent layer of smaller MNPs under some larger agglomerations of non-biotemplated particles formed in the bulk solution. Scale bars: (d) 20 μm, (a & e) 2 μm, (b, c & f) 200 nm.

erature is essential to ensuring that MNPs are formed by the cys_CoPt peptide. Mineralising at 18 °C allowed the biotemplating peptide to consistently form uniform MNPs on the substrates. Fig. S4‡ shows a surface biomineralised at 35 °C, where the biotemplating peptide forms an inconsistent layer of non-particulate material. At temperatures between these values, inconsistent non-continuous films are formed by the immobilised biotemplating peptide. Thus all mineralisation was optimised at 18 °C to form a monolayer of MNPs.

CoPt MNPs are biotemplated on patterned surfaces

Surface biotemplated particle size and shape ideal for single domain L1$_0$ CoPt. Biotemplated surfaces were imaged using

SEM, and analysed to determine grainsize and shape distributions (Fig. 3 and Table 1). The surface biotemplated MNPs have a suitable size (*i.e.* single domain, which is between
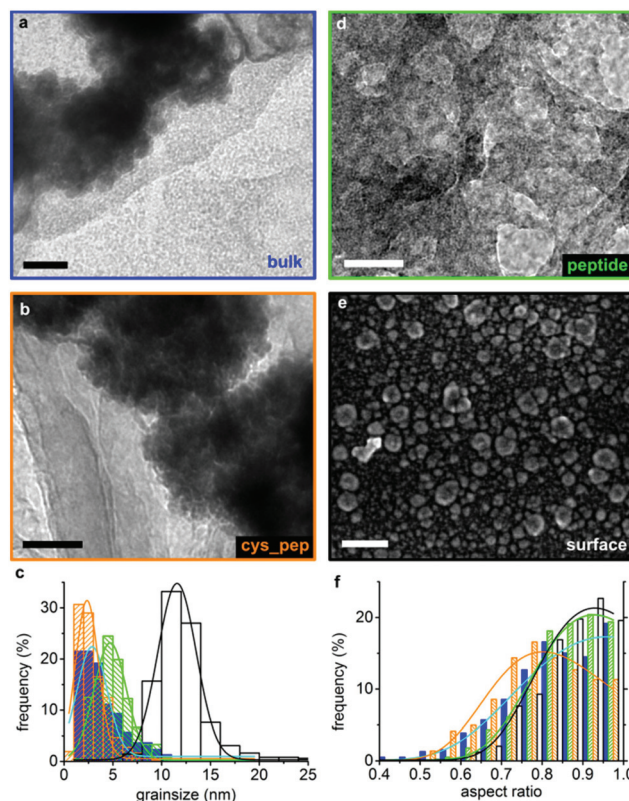

Fig. 3 Electron microscopy and grainsize analysis of surface biotemplated CoPt and appropriate controls. Transmission electron microscopy (TEM) images of (a) particles precipitated from a bulk solution in the absence of a biotemplating peptide (blue), (b) in the presence of the biotemplating peptide (green) and (d) the cys_CoPt peptide (orange). (e) Scanning electron microscope (SEM) image of the patterned biotemplated surface showing a lines pattern (black). Larger particles on the surface are agglomerations of smaller MNPs, likely to be magnetically attracted to the biotemplated thin-film. (c) Grainsize distribution graph fitted with Gaussian distributions and (f) aspect ratio fitted with Extreme fit in Origin Pro. Scale bars (a, b & d) 20 nm and (e) 200 nm.

Table 1 Summary of grainsize and shape analysis data for surface biotemplated particles, and controls of bulk precipitated non-biotemplated, peptide biotemplated and cysteine tagged peptide biotemplated MNPs. About 400 particles were measured in Image J[55] for each sample. Grainsize is the peak of a Gaussian distribution fitted to the measured data, and the error is the full width at half maximum of this curve. The aspect ratio is the shortest axis divided by the longest axis (width/length), and the error is one standard deviation of the data

Sample name	Grainsize (nm)	Error± (nm)	Aspect ratio	Error
Bulk	3	3	0.83	0.12
CoPt peptide	5	3	0.86	0.09
cys_CoPt peptide	2	2	0.80	0.12
Surface cys_CoPt peptide	12	4	0.87	0.09

5 [11,53] and 100 nm [54] for L1$_0$ CoPt) and narrow dispersity (12 ± 4 nm). We speculate that the close packing of a CoPt biotemplating peptide onto a surface helps to biotemplate uniformly sized MNPs during metallisation.[38,43] The cys_CoPt peptide (16 amino acids) is smaller than the silicon binding dual affinity peptide (DAP) used previously[43,48] (27 amino acids). This means that the cys_CoPt peptide should be able to pack more closely on a surface than the DAP. This higher surface density of peptide could enhance the templating of smaller, more uniform MNPs (12 ± 4 nm) when compared to DAP-templated particles (17 ± 9 nm).[43] The surface biotemplated particles are also the most equidimensional of all the samples analysed (aspect ratio (AR) 0.87 ± 0.09, see Table 1).

Control particles were formed from a bulk solution with no biotemplate (bulk), and in the presence of 10 μg mL^{-1} of the cys-tagged peptide (cys_CoPt peptide, CGSGKTHEIHSPLLHK) and a non-cys-tagged version (CoPt peptide, GSGKTHEIHSPLLHK). Bulk precipitated particles have a broad size distribution (3 ± 3 nm) and are slightly more elongated than the surface templated MNPs (AR 0.83 ± 0.12, Fig. 3). The bulk particles agglomerate into clumps, and this self-assembly is probably driven by their broad grainsize distribution.[56] The cys_CoPt peptide formed the smallest (2 ± 2 nm) and most elongated (0.80 ± 0.12) particles. The CoPt peptide biotemplated slightly larger particles with a narrower distribution (5 ± 3 nm) and a more equidimensional shape (AR 0.86 ± 0.09). Cysteine is known to biotemplate metallic nanoparticles,[57,58] so the addition of this one amino acid would be expected to alter the biotemplating action of the CoPt peptide when the cysteine is exposed and free in solution. All the bulk precipitated particles were smaller than the superparamagnetic grainsize limit (i.e. ≈5 nm)[11] for L1$_0$ CoPt, and have a broader grainsize distribution than those biotemplated by the cys_CoPt immobilised on the gold surface. This clearly demonstrates that the immobilisation of the cys_CoPt biotemplating peptide onto a substrate enhances its ability to control the formation of more uniform, single domain sized MNPs when compared to the peptide in a bulk solution.

Elemental composition shows MNPs contain Co and Pt. Energy dispersive X-ray (EDX) analysis was used to probe the elemental composition of the MNPs biotemplated onto the surface (Fig. 4) and the powder controls (Fig. S5‡). The EDX maps in Fig. 4d show that platinum is co-localised onto the line patterns within the biotemplated particles. The spectrum from the biotemplated surface shows a peak at 0.78 keV from Co Lα, and a shoulder on the Au Lα peak at 9.41 keV, which we assign to Pt Lα (Fig. 4e). Due to the overlap of the Au Lα and Pt Lα peaks, it was impossible to quantify the ratio of Co : Pt, as the abundance of Pt is overestimated by the fitting (≈5 : 7 Co : Pt). In our previous work[43] using this biotemplating CoPt sequence on a silicon surface, EDX showed a 1 : 1 ratio of Co : Pt in the surface biotemplated MNPs using these reaction conditions. Therefore it is likely that stoichiometric CoPt rather than CoPt$_3$ is biotemplated by the cys_CoPt peptide on the surface.

The spectra show the expected peaks that are due to the glass substrate (Kα lines for Si, O, Na, Mg, Cl, and Ca), the de-
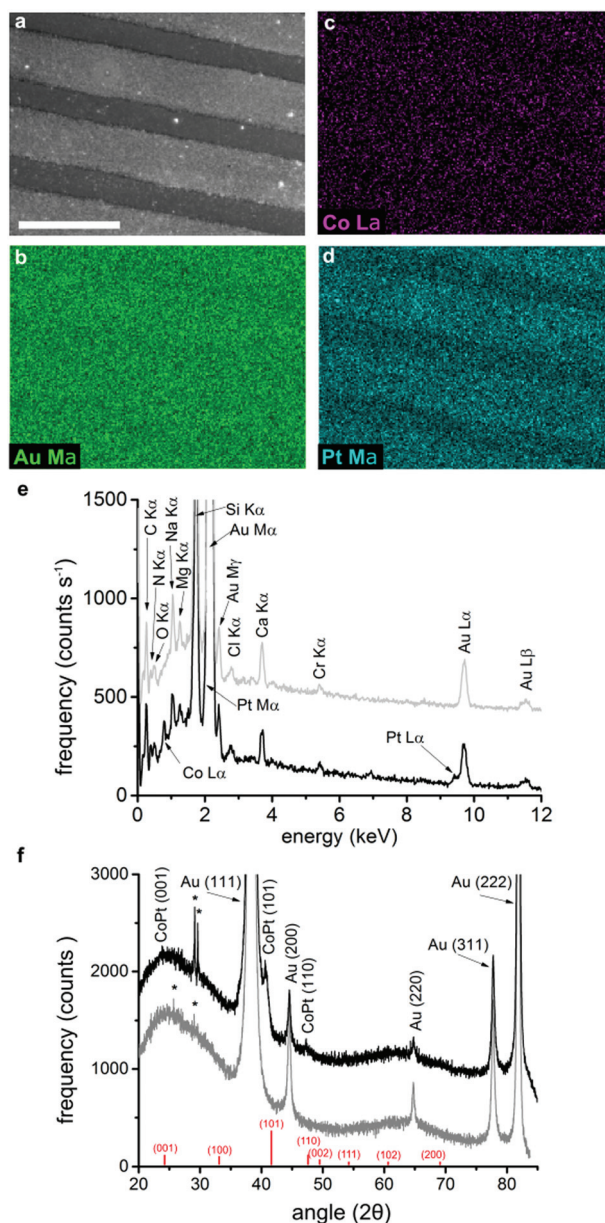

Fig. 4 Electron microscopy, energy dispersive X-ray (EDX) maps and spectra, and X-ray Diffraction (XRD) spectra of the biotemplated patterned surface. (a) SEM image of a biotemplated patterned surface (scale bar 20 μm). Maps show the relative abundances of (b) gold, (c) cobalt and (d) platinum of the area shown in (a) (recorded at 15 keV). (e) EDX spectra and (f) XRD spectra from the biomineralised part of the pattern (black) and the non-biomineralised part of the surface (grey). The peaks indicated with asterisks (*) are a good match for carbon (e.g. see Wang et al.).[72] Spectra are offset vertically to show the reflections more clearly. CoPt peak positions are labelled in red (intensity represented by height of red line), and peak positions and assignments are summarised in Table S1.‡

posited metal film (Au Mα, Mγ, Lα and Lβ; and Cr Kα), and from adsorbed organics (Kα lines for C, N and O). The EDX spectra of the powder controls (Fig. S5‡), show contributions from the nanoparticles (Co Lα, Co Kα, Co Kβ, Pt Mα, Pt Mγ,

Pt Lα and Pt Lβ) and the TEM grid (Cu, Si, O and C) as expected. This demonstrates that the biotemplating cys_CoPt peptide is able to biotemplate particles containing Co and Pt onto the patterned surfaces.

Crystallography indicates some L1₀ ordering. The crystallinity of the biotemplated surfaces and the powder controls were probed using X-ray diffraction (XRD) (Fig. 4f & S6 and Table S1‡) and selected area electron diffraction (SAED) (Fig. S7 and Table S2‡). The biotemplated surface has peaks at $2\theta = 23.99°$, $40.79°$ and $47.51°$, which correspond most closely to the CoPt L1₀ (001), (101) and (110) planes respectively (Table S1‡). The relevant CoPt₃ (100), (110) and (111) planes are not as close to the measured values. Also, the EDX data (which overestimates the amount of Pt present) shows a ratio of $\approx 5 : 7$ Co : Pt. This is much closer to the value required for CoPt (1 : 1) than for CoPt₃ (1 : 3). Thus we have tentatively assigned these peaks as L1₀ CoPt. A gold coated glass substrate shows a broad XRD peak between $2\theta \approx 20°$–$30°$, which we attribute to the silica glass slide, and peaks at $2\theta = 38.30°$, $44.56°$, $64.78°$, $77.77°$ and $81.82°$, which are assigned as the FCC Au (111), (200), (220), (311) and (222) reflections respectively. If present, the low coercivity A1 phase of CoPt would show (111), (200) and (220) peaks,[9] which are not observed in our surface biotemplated CoPt.

High temperature annealing (650 °C) of sputtered CoPt is needed to create the long-range order necessary to achieve high coercivity L1₀ CoPt thin-films with c-axis aligned out-of-plane. This would be indicated by the presence of (001) and (100) peaks, splitting of the (200) peak to reveal the (220) plane,[9,59] and the absence of the A1 CoPt (111) peak.[8] The surface biotemplated MNPs show the (001), (101) and (110) planes, and lack a CoPt A1 (111) peak, which indicates that they have some L1₀ features. It is possible that the action of the surface immobilised peptide is able to direct the crystallisation of stoichiometric CoPt by lowering the activation energy of the formation of this phase. It is probable that the MNPs are orientated randomly (i.e. there is a lack of long-range L1₀ ordering).[60] This may be why we observe different L1₀ CoPt planes (i.e. (001), (101) and (110)) to those seen in the c-axis aligned annealed samples (i.e. (001), (110), (200) and (220)).[8,9] If a biotemplating peptide was able to order the MNPs in a particular crystallographic orientation, it would offer tremendous promise for finding conditions that are able to achieve out-of-plane c-axis alignment of biotemplated L1₀ CoPt.

SAED (Fig. S7 and Table S2‡), showed no L1₀ structure for any of the bulk templated particles. XRD on these bulk templated particles (Fig. S6 and Table S1‡) show peaks at $2\theta \approx 40.6°$, $47.1°$ and $69.0°$, which correspond to the (111), (200) and (220) planes of CoPt₃. This highlights how attachment of the cys_CoPt to a gold surface significantly improves the formation of stoichiometric CoPt over other phases for these reaction conditions. These diffraction data demonstrate that the surface bound cys_CoPt is able to template the formation of stoichiometric CoPt from aqueous solution at 18 °C, but is not able to order the c-axis out-of-plane.

Magnetic studies of surface biotemplated CoPt

Whole sample magnetic measurements show ferromagnetism. The magnetic response of surface biotemplated MNP films was measured using vibrating sample magnetometry (VSM) (Fig. S8‡) and magneto-optical Kerr effect (MOKE) magnetometry (Fig. S9‡). Both VSM and MOKE measurements show a ferromagnetic hysteresis at room temperature with a coercivity of 20–30 Oe, whether measured in-plane or out-of-plane. High coercivity of L1₀ CoPt is achieved by c-axis alignment perpendicular to the surface.[8,9] Therefore, our biotemplated films must lack this alignment, so have low coercivity. We also observe no increase in coercivity for surfaces biomineralised with CoPt in the presence of a 0.2 T DC field, whether applied perpendicularly or parallel to the surface (Fig. S10 & S11‡), and MOKE measurements on these samples showed no improvement in coercivity. A lack of long-range L1₀ ordering may also be why we observe the (101) and (110) L1₀ CoPt reflections in the biotemplated films, rather than the (001), (100), (200), and (220) peaks seen in annealed thin-films.[9]

Nano-scale magnetism probed using MFM. Magnetic force microscopy (MFM) of the patterned biotemplated MNPs (Fig. 5, & S12–S19‡) reveal that the patterned areas protected by the PEG to resist MNP biotemplating do not show any magnetic interactions between the tip and the surface as expected. Magnetic interactions between the magnetised tip and the MNPs on the nano-patterned surfaces are mainly repulsive (Fig. 5a & b and S12‡). This is likely to be due to the MNPs on the surfaces being magnetised in the same direction as the probe, thus they repel the tip. Despite using lift heights above the height of the MNP topography, it is difficult to discount that interactions of the topography with the magnetised tip may also be responsible for the phase contrast in the nano-patterned samples. Thus, we also studied the magnetism of the micro-patterned surfaces, where the pattern scale is much larger than the MNP size.

On the µCP patterns, the closely packed MNPs appear to combine into a complex magnetic domain structures. These domains appear to be aligned preferentially in the same direction as the micro-patterned lines when observed over a range of length scales (Fig. 5c & d and S13‡) and they remain in the same place when the scan size was reduced and/or the direction was rotated (Fig. S14–S17‡). The presence of stable domains when the scan size and direction is altered indicates that this phase contrast is independent of the surface topography, i.e. the phase contrast is due to magnetic and not other physical interactions between the magnetised tip and the surface.

These domains indicate that the magnetic alignment of the particles is stable at room temperature, which is promising for their use in spin-ice, sensing, cell sorting, cell manipulation and data storage applications. Multi-particle magnetic domains that align with the macroscopic shape of an assembly of MNPs has been observed previously using MFM,[30,31] and in Fresnel–Lorentz microscopy and electron holography.[61] The size and shape of these domains are likely to be strongly dependent on the packing of MNPs within the film,[62] i.e. the
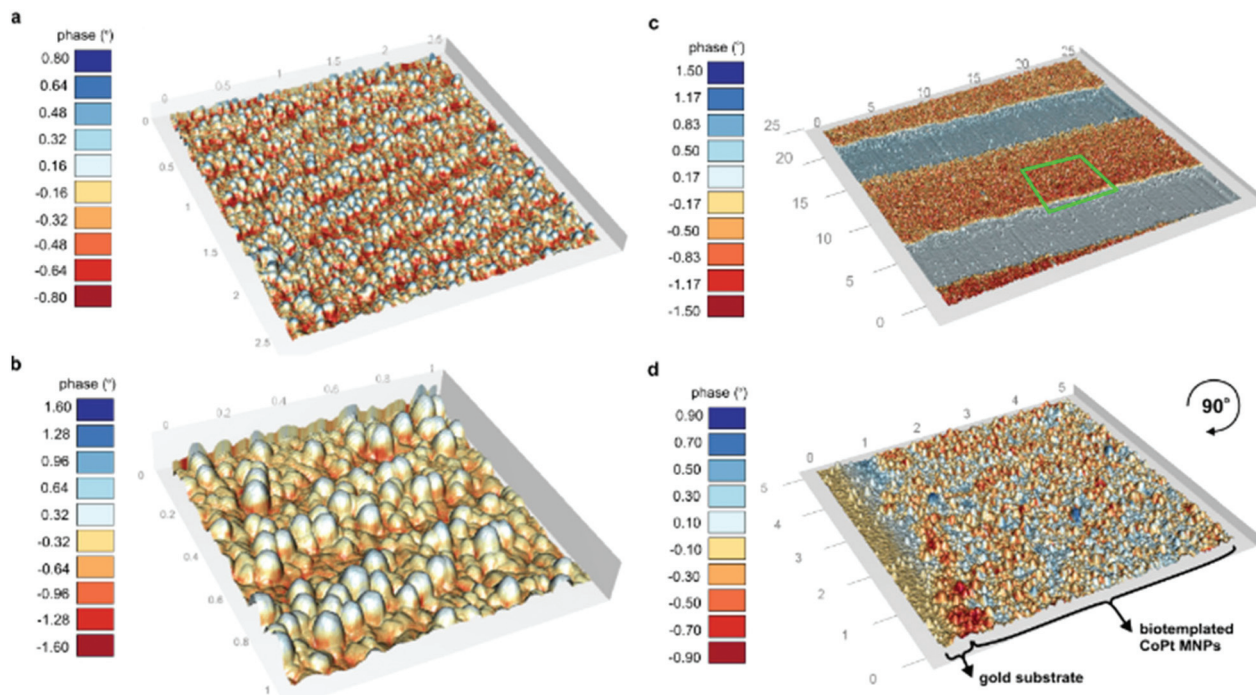
Fig. 5 MFM plots of biotemplated CoPt patterned surface (separate plots show in Fig. S12 & S13‡). A negative phase shift indicates attraction (red) between the tip and the surface, and a positive phase shift indicates repulsion (blue). The topography is recorded in tapping mode and the phase shift recorded at a lift height of 50 nm (a) 2.5 μm^2 scan area surface and (b) 1 μm^2 of IL nano-patterned biotemplated CoPt. (c) 25 μm^2 and (d) 5 μm^2 scan area of μCP micro-patterned biotemplated CoPt surface. Green area in (c) highlights the location scanned for plot (d). 5 μm^2 scan area recorded at a 90° angle to image (c). These IL and μCP surfaces show zones of attraction and repulsion that extend across multiple MNPs on the surface.

domain alignment may be due to demagnetising effects resulting from the patterning. In the absence of any patterning, the surface biotemplated MNPs exhibited domain patterns with no preferred directionality (Fig. S18 & S19‡) but with larger domains than on the micro-patterned MNP films. There is no evidence of multi-particle zones of magnetic attraction or repulsion from nano-patterned surfaces. This may be due to the shape anisotropy of the IL nano-patterned lines enhancing the alignment of the biotemplated MNPs when compared to the μCP patterns.

Conclusions and future outlook

We have demonstrated that peptides can be used to biotemplate a technologically relevant magnetic material onto nano- and micro-patterned surfaces. Our biotemplating cys_CoPt peptide has excellent control over particle size to form a consistent magnetic thin-film, and our surface biotemplated CoPt MNPs are above the superparamagnetic size limit for the $L1_0$ phase. The coercivity of the biotemplated particles is too low for recording. However, these patterned magnetic soft thin-films have extensive applicability for sorting and manipulating cells and magnetic beads,[1,2] in sensors,[3,4] and in studying 2D spin-ices.[5,6] Sputtered $L1_0$ platinum alloys show extremely high coercivity,[8,10] which is due to out-of-plane c-axis alignment of the MNPs. Therefore, further work is required to perpendicu-

larly align the c-axis to increase the coercivity of these biotemplated MNPs if we are to develop biotemplated BPM. Previously, annealing was shown to improve the coercivity of biotemplated Pt alloy MNPs.[36,38,42,63] However, annealing can lead to agglomeration, which could adversely affect the magnetic properties of the biotemplated films. Also, we believe that annealing the biotemplated samples would be counter-productive, as adding high temperature processing steps removes the advantages afforded by using biotemplating; such as low cost, low temperature and low energy processing. Therefore, we propose a number of potential improvements to be explored in the future development of biotemplated $L1_0$ CoPt.

We have used a short, cysteine tagged biotemplating peptide sequence (CGSGKTHEIHSPLLHK). In previous work,[43] our DAP peptide (which is the CoPt biotemplating sequence appended to a silicon binding motif 'spacer'), biotemplated larger particles under similar biomineralisation conditions. Therefore, it is likely that adding a longer spacer between the cysteine and the CoPt biotemplating sequence would also biomineralise larger MNPs. Equally, adding repeats of the biomineralisation sequence could create smaller biotemplated MNPs by more closely packing the CoPt peptide onto the surface. Thus, it may be possible to control the grainsize of the biotemplated MNPs by altering the spacer length and the number of biomineralisation motif repeats. However, as the cys_CoPt peptide was unable to align the c-axis of the biotemplated MNPs to create the high coercivity necessary for data

storage, we feel that this would be more important to address in the immediate future.

Neither a perpendicular nor parallel DC field of 0.2 T was able to align the CoPt MNPs during mineralisation. Increasing the field strength and/or using an alternating field could introduce the desired alignment of $L1_0$ CoPt. There are biotemplating peptides that interact with specific mineral facets to effect nanoparticle shape control.[41,64–67] Thus, it should also be possible to modify or develop a biotemplating peptide to form out-of-plane c-axis aligned $L1_0$ CoPt. However, the interaction between biotemplating peptides and specific crystal facets is currently poorly understood, even for simple monometallic systems.[41,64–67] Therefore, designing a biotemplating peptide for the more complex bimetallic $L1_0$ CoPt phase, with a c-axis alignment in a specific orientation, is an ambitious future project. The biomineralisation and patterning methodology presented here could be adapted to both immobilise and pattern such a biotemplating sequence to produce crystallographically aligned biotemplated BPM in the future.

In this work, we have combined top-down soft- and photolithographic patterning with bottom up self-assembly of biotemplating molecules to create nano- and micro-scale patterns of MNPs in an environmentally benign manner. As such, we have demonstrated the adaptability of our process towards the production of patterns across a range of length scales, and with a variety of morphologies. Most pleasingly, no high temperature or other energy intensive processing is needed to create these biotemplated arrays of CoPt, making this a truly environmentally friendly method of manufacturing magnetic thin-films that could be used in applications.

There is an unimaginable myriad of biological molecules and systems that could be adapted and combined to make industrially and technologically relevant materials.[14,16] Current research has demonstrated that biomimetic and biokleptic materials can be used to build photovoltaics,[68] electronic circuits,[69] fibre optics,[26] optical displays,[70] and magnetic thin-films (this work and Galloway *et al.*).[43] Our biomineralisation nano- and micro-patterning strategies presented here could be extended and adapted to create patterns of these other useful biotemplated materials to build such components. These individual components could then be combined to produce bioinspired versions of everyday consumer devices such as smartphones or laptops. Our work on developing patterned biotemplated magnetic thin-films is an important step in enabling us to manufacture such bioinspired devices in the future.

Experimental

Extended experimental methods are available in the ESI.‡

Sample preparation

Nano-patterning using interference lithography (IL). A SAM was formed on clean gold surfaces by immersion in an alkanethiol solution (1 mM 11-mercaptoundecyl tetra(ethylene) glycol (PEG) in ethanol) for 24 hours. SAM nano-patterning was performed using a Coherent Innova 300C FreD frequency doubled argon ion laser beam ($\lambda \approx 244$ nm, maximum power 100 mW) in a Lloyd's mirror arrangement.[49] The laser beam was expanded to illuminate area of ≈ 1 cm^2, and was directed towards the surface at a fixed angle of 2θ to the mirror. The SAMs were exposed to a dose of 20–40 J cm^{-2}, resulting in spatially defined nano-scale photo-oxidation of the SAM on the gold surface.

Micro-contact printing (µCP). Patterned silicon masters were cleaned with propanol and dried with N_2. Poly dimethyl siloxane (PDMS, Sylguard 184 base with w/w 10% curing agent) was poured on, and the bubbles removed under vacuum. The PDMS was cured (16 hours, 60 °C) before the stamps were cut out and soaked in ethanol (16 hours). Stamps were dried with N_2 and inked with 5 mM PEG in ethanol for 4 minutes. Stamps were dried under N_2 prior to micro-contact printing (µCP) onto clean gold films by conformal contact for 4 minutes.

Peptide functionalisation of a surface. A clean gold surface (unpatterned), a micro-contact printed surface (µCP,) or an interference lithographically patterned surface (IL) was immersed in a solution of 20 µg mL^{-1} of the cys_CoPt peptide (CGSGKTHEIHSPLLHK, Genscript, >95% purity) in phosphate buffered saline (PBS from Invitrogen: 10 mM sodium phosphate, 2.68 mM KCl, 140 mM NaCl, pH 7.4). After 1 hour, the substrates were rinsed in water and placed into a mineralisation vessel.

Biotemplated mineralisation. Solutions of cobalt sulfate (Co^{2+}, 30 mM CoSO$_4$·7H$_2$O, 126.5 mg in 15 mL) and sodium tetrachloroplatinate (Pt^{2+}, 10 mM Na$_2$PtCl$_4$, 57.4 mg in 15 mL) salts were prepared in deoxygenated MilliQ water (vacuum degassed for >1 hour and sparged with N_2 gas for >1 hour). 2.5 mL Co^{2+} and 2.5 mL Pt^{2+} were added to the peptide patterned gold substrate and incubated at 18 °C. For the bulk peptide control, 100 µL of a 1 mg mL^{-1} peptide solution (10 µg mL^{-1} in the 10 mL reaction) in PBS was added in place of the peptide patterned substrate. N_2 was flowed through the solutions for the duration of the mineralisation. Sodium borohydride (25 mM, NaBH$_4$, 28.5 mg in 30 mL) was then prepared in deoxygenated water. After 5 minutes, 5.0 mL of NaBH$_4$ was injected into the reaction vessel. Surfaces were removed after ≈ 45 minutes, and rinsed 3–5 times in deoxygenated water and dried with N_2.

Characterisation

Electron microscopy. A Hitachi SU8230 cold field emission scanning electron microscope (SEM) was used to image samples at 2–15 keV *via* the in-lens SE(U) detector. Energy dispersive X-ray (EDX) spectra were recorded using an Oxford Instruments AZtecEnergy EDX system at 15 keV. A Phillips CM200(FEG)TEM (transmission electron microscope) was used to image bulk precipitated samples on carbon coated copper grids at 200 keV, using the digital micrograph software. EDX spectra were recorded using an Oxford Instruments INCA EDX

system and Gatan Imaging Filter. ImageJ [55] was used to record the line pattern widths and the length and width of the MNPs.

X-ray diffraction (XRD). A Brucker-AXS D8 series2 diffractometer set to a Bragg Brentano Parafocussing Geometry was used to record diffraction spectra. X-rays were generated using a Cu Kα source at 40 kV at room temperature. Monochromated X-rays were passed through a 2 mm exit slit and an automatic divergence slit of 0.2°. Diffraction intensity was collected at 2θ between 2° and 80° on a Braun position sensitive detector (0.02° and 6.0 seconds per step). These data were processed using AXS Commander and EVA software.

Vibrating sample magnetometry (VSM). Hysteresis loops were measured with a field applied perpendicular and parallel to the surface with a Microsense Model 10 vector VSM, using an applied field of −5 to 5 kOe at 295 K.

Magneto-optical Kerr effect (MOKE). Measurements were taken in the polar and longitudinal geometries. A HeNe laser (λ = 633 nm) was directed through a polariser onto the sample at an incident angle of 0° (polar) or ≈30° (longitudinal) from the surface normal. A magnetic field of up to 6 kOe was applied out-of-plane (polar) or at any angle in the plane (longitudinal).

Magnetic force microscopy (MFM). Force microscopy plots were recorded using MFM tips (Cr/Co coated MESP probes, Brucker). Tips were magnetised then mounted onto the piezo-head of a Multimode Nanoscope III. The surface topography was recorded in tapping mode. This height trace was then followed at a lift height above the height of the particles (30–50 nm). These MFM data were processed using WSxM [71] and Nanoscope Analysis v1.50, and 3D plots generated in 'R' using the rgl package (script available at: https://github.com/jonbramble/MFMPlot).

Author contributions

JMG designed the investigation in consultation with KC, JJM and SSS. JMG also designed the biotemplating peptide, optimised mineralisation protocols, prepared micro-patterned biotemplated substrates, imaged samples using electron microscopy, recorded and analysed spectra using EDX, analysed XRD data, collected and processed MFM data, and wrote the manuscript. SMB made stamp masters for µCP, helped to optimise the biomineralisation of surfaces and performed SEM and MFM, and made IL nano-patterns with OE-Z and GJL. JET co-ordinated VSM with JJM. PMS recorded and analysed MOKE data. RCB performed mineralisation in an applied field and MOKE measurements with JMG, SMB and DAA. All authors discussed the direction of the project and the results, and contributed to writing and editing the manuscript.

Acknowledgements

Notes and references

1 L. V. Cuong, N. X. Nghia and P. D. Thang, *Mater. Trans.*, 2015, **56**, 1431–1433.

2 M. T. Bryan, K. H. Smith, M. E. Real, M. A. Bashir, P. W. Fry, P. Fischer, M. Y. Im, T. Schrefl, D. A. Allwood and J. W. Haycock, *IEEE Magn. Lett.*, 2010, **1**, 1500104.

3 L. Jogschies, D. Klaas, R. Kruppe, J. Rittinger, P. Taptimthong, A. Wienecke, L. Rissing and M. C. Wurz, *Sensors*, 2015, **15**, 28665–28689.

4 H. Corte-León, V. Nabaei, A. Manzin, J. Fletcher, P. Krzysteczko, H. W. Schumacher and O. Kazakova, *Sci. Rep.*, 2014, **4**, 6045.

5 R. F. Wang, C. Nisoli, R. S. Freitas, J. Li, W. McConville, B. J. Cooley, M. S. Lund, N. Samarth, C. Leighton, V. H. Crespi and P. Schiffer, *Nature*, 2006, **439**, 303–306.

6 J. P. Morgan, A. Stein, S. Langridge and C. H. Marrows, *Nat. Phys.*, 2011, **7**, 75–79.

7 T. R. Albrecht, H. Arora, V. Ayanoor-Vitikkate, J. Beaujour, D. Bedau, D. Berman, A. L. Bogdanov, Y. Chapuis, J. Cushen, E. E. Dobisz, G. Doerk, H. Gao, M. Grobis, B. Gurney, W. Hanson, O. Hellwig, T. Hirano, P. Jubert, D. Kercher, J. Lille, Z. Liu, C. M. Mate, Y. Obukhov, K. C. Patel, K. Rubin, R. Ruiz, M. Schabes, L. Wan, D. Weller, T. Wu and E. Yang, *IEEE Trans. Magn.*, 2015, **51**, 1–42.

8 L. Zhang, Y. K. Takahashi, K. Hono, B. C. Stipe, J.-Y. Juang and M. Grobis, *J. Appl. Phys.*, 2011, **109**, 07B703.

9 L. N. Yu, L. Y. Lu, Z. D. Xu, X. G. Xu, J. Miao and Y. Jiang, *Mater. Lett.*, 2012, **86**, 142–145.

10 O. Mosendz, S. Pisana, J. W. Reiner, B. Stipe and D. Weller, *J. Appl. Phys.*, 2012, **111**, 07B729.

11 X. Sun, Z. Y. Jia, Y. H. Huang, J. W. Harrell, D. E. Nikles, K. Sun and L. M. Wang, *J. Appl. Phys.*, 2004, **95**, 6747–6749.

12 O. Hellwig, A. Berger, T. Thomson, E. Dobisz, Z. Z. Bandic, H. Yang, D. S. Kercher and E. E. Fullerton, *Appl. Phys. Lett.*, 2007, **90**, 162516.

13 S. Mann, *Biomineralization: Principals and Concepts in Bioinorganic Materials Chemistry*, Oxford University Press, Oxford, UK, 2001.

14 F. Nudelman and N. A. J. M. Sommerdijk, *Angew. Chem., Int. Ed.*, 2012, **51**, 6582–6596.

15 J. M. Galloway and S. S. Staniland, *J. Mater. Chem.*, 2012, **22**, 12423–12434.

16 J. M. Galloway, J. P. Bramble and S. S. Staniland, *Chem. – Eur. J.*, 2013, **19**, 8710–8725.

17 F. C. Meldrum and H. Cölfen, *Chem. Rev.*, 2008, **108**, 4332–4432.

18 G. E. Fantner, O. Rabinovych, G. Schitter, P. Thurner, J. H. Kindt, M. M. Finch, J. C. Weaver, L. S. Golde, D. E. Morse, E. A. Lipman, I. W. Rangelow and P. K. Hansma, *Compos. Sci. Technol.*, 2006, **66**, 1205–1211.

19 J. C. Weaver, G. W. Milliron, P. Allen, A. Miserez, A. Rawal, J. Garay, P. J. Thurner, J. Seto, B. Mayzel, L. J. Friesen, B. F. Chmelka, P. Fratzl, J. Aizenberg, Y. Dauphin, D. Kisailus and D. E. Morse, *J. Adhes.*, 2010, **86**, 72–95.

20 M. Hildebrand, *Chem. Rev.*, 2008, **108**, 4855–4874.

21 C. T. Lefèvre and D. A. Bazylinski, *Microbiol. Mol. Biol. Rev.*, 2013, **77**, 497–526.

22 A. Arakaki, H. Nakazawa, M. Nemoto, T. Mori and T. Matsunaga, *J. R. Soc., Interface*, 2008, **5**, 977–999.

23 T. Prozorov, D. A. Bazylinski, S. K. Mallapragada and R. Prozorov, *Mater. Sci. Eng., R*, 2013, **74**, 133–172.

24 L. Addadi and S. Weiner, *Phys. Scr.*, 2014, **89**, 98003.

25 Y.-Y. Kim, L. Ribeiro, F. Maillot, O. Ward, S. J. Eichhorn and F. C. Meldrum, *Adv. Mater.*, 2010, **22**, 2082–2086.

26 J. Aizenberg, V. C. Sundar, A. D. Yablon, J. C. Weaver and G. Chen, *Proc. Natl. Acad. Sci. U. S. A.*, 2004, **101**, 3358–3363.

27 A. R. Muxworthy, W. Williams, A. P. Roberts, M. Winklhofer, L. Chang and M. Pósfai, *Geochem., Geophys., Geosyst.*, 2013, **14**, 5430–5441.

28 X. Liu, H. Zhang, S. Nayak, G. Parada, J. Anderegg, S. Feng, M. Nilsen-Hamilton, M. Akinc and S. K. Mallapragada, *Ind. Eng. Chem. Res.*, 2015, **54**, 10284–10292.

29 A. Arakaki, F. Masuda and T. Matsunaga, *Mater. Res. Soc. Proc.*, 2009, **1187**, KK03–KK08.

30 J. M. Galloway, J. P. Bramble, A. E. Rawlings, G. Burnell, S. D. Evans and S. S. Staniland, *Small*, 2012, **8**, 204–208.

31 J. M. Galloway, J. P. Bramble, A. E. Rawlings, G. Burnell, S. D. Evans and S. S. Staniland, *J. Nano Res.*, 2012, **17**, 127–146.

32 S. M. Bird, O. El-Zubir, A. E. Rawlings, G. J. Leggett and S. S. Staniland, *J. Mater. Chem. C*, 2016, **4**, 3948–3955.

33 S. M. Bird, A. E. Rawlings, J. M. Galloway and S. S. Staniland, *RSC Adv.*, 2016, **6**, 7356–7363.

34 J. M. Galloway, A. Arakaki, F. Masuda, T. Tanaka, T. Matsunaga and S. S. Staniland, *J. Mater. Chem.*, 2011, **21**, 15244–15254.

35 S. M. Bird, J. M. Galloway, A. E. Rawlings, J. P. Bramble and S. S. Staniland, *Nanoscale*, 2015, **7**, 7340–7351.

36 B. D. Reiss, C. Mao, D. J. Solis, K. S. Ryan, T. Thomson and A. M. Belcher, *Nano Lett.*, 2004, **4**, 1127–1132.

37 M. Sarikaya, C. Tamerler, A. K. Y. Jen, K. Schulten and F. Baneyx, *Nat. Mater.*, 2003, **2**, 577–585.

38 C. Mao, D. J. Solis, B. D. Reiss, S. T. Kottmann, R. Y. Sweeney, A. Hayhurst, G. Georgiou, B. Iverson and A. M. Belcher, *Science*, 2004, **303**, 213–217.

39 R. R. Naik, S. E. Jones, C. J. Murray, J. C. McAuliffe, R. A. Vaia and M. O. Stone, *Adv. Funct. Mater.*, 2004, **14**, 25–30.

40 M. B. Dickerson, R. R. Naik, M. O. Stone, Y. Cai and K. H. Sandhage, *Chem. Commun.*, 2004, 1776–1777.

41 C.-Y. Chiu, Y. Li, L. Ruan, X. Ye, C. B. Murray and Y. Huang, *Nat. Chem.*, 2011, **3**, 393–399.

42 M. T. Klem, D. Willits, D. J. Solis, A. M. Belcher, M. Young and T. Douglas, *Adv. Funct. Mater.*, 2005, **15**, 1489–1494.

43 J. M. Galloway, J. E. Talbot, K. Critchley, J. J. Miles and J. P. Bramble, *Adv. Funct. Mater.*, 2015, **25**, 4590–4600.

44 J. Kim, Y. Rheem, B. Yoo, Y. Chong, K. N. Bozhilov, D. Kim, M. J. Sadowsky, H.-G. Hur and N. V. Myung, *Acta Biomater.*, 2010, **6**, 2681–2689.

45 S. Brown, *Nat. Biotechnol.*, 1997, **15**, 269–272.

46 R. R. Naik, S. J. Stringer, G. Agarwal, S. E. Jones and M. O. Stone, *Nat. Mater.*, 2002, **1**, 169–172.

47 C. E. Flynn, C. Mao, A. Hayhurst, J. L. Williams, G. Georgiou, B. Iverson and A. M. Belcher, *J. Mater. Chem.*, 2003, **13**, 2414–2421.

48 J. M. Galloway, S. M. Bird, J. P. Bramble, K. Critchley and S. S. Staniland, in *MRS Spring*, San Francisco, USA, 2013, vol. 1569, pp. 231–237.

49 G. Tizazu, O. El-Zubir, S. R. J. Brueck, D. G. Lidzey, G. J. Leggett and G. P. Lopez, *Nanoscale*, 2011, **3**, 2511–2516.

50 A. Kumar and G. M. Whitesides, *Appl. Phys. Lett.*, 1993, **63**, 2002–2004.

51 M. Mrksich and G. M. Whitesides, *Trends Biotechnol.*, 1995, **13**, 228–235.

52 N. L. Jeon, R. G. Nuzzo, Y. Xia, M. Mrksich and G. M. Whitesides, *Langmuir*, 1995, **11**, 3024–3026.

53 B. Varghese, S. N. Piramanayagam, Y. Yang, S. Kai Wong, H. Khume Tan, W. Kiat Lee and I. Okamoto, *J. Appl. Phys.*, 2014, **115**, 17B707.

54 S. H. Liou, Y. Liu, S. S. Malhotra, M. Yu and D. J. Sellmyer, *J. Appl. Phys.*, 1996, **79**, 5060–5062.

55 M. D. Abramoff, P. J. Magalhaes and S. J. Ram, *Biophotonics Int.*, 2004, **11**, 36–42.

56 Y. Xia, T. D. Nguyen, M. Yang, B. Lee, A. Santos, P. Podsiadlo, Z. Tang, S. C. Glotzer and N. A. Kotov, *Nat. Nanotechnol.*, 2011, **6**, 580–587.

57 T. Nishinaka, A. Takano, Y. Doi, M. Hashimoto, A. Nakamura, Y. Matsushita, J. Kumaki and E. Yashima, *J. Am. Chem. Soc.*, 2005, **127**, 8120–8125.

58 T. Scheibel, R. Parthasarathy, G. Sawicki, X.-M. Lin, H. Jaeger and S. L. Lindquist, *Proc. Natl. Acad. Sci. U. S. A.*, 2003, **100**, 4527–4532.

59 M. S. Wellons, Z. Gai, J. Shen, J. Bentley, J. E. Wittig and C. M. Lukehart, *J. Mater. Chem. C*, 2013, **1**, 5976–5980.

60 M. Yu, H. Ohguchi, A. Zambano, I. Takeuchi, J. P. Liu, D. Josell and L. A. Bendersky, *Mater. Sci. Eng., B*, 2007, **142**, 139–143.

61 K. Yamamoto, C. R. Hogg, S. Yamamuro, T. Hirayama and S. A. Majetich, *Appl. Phys. Lett.*, 2011, **98**, 72509.

62 J. J. Miles, *IEEE Trans. Magn.*, 2007, **43**, 955–967.

63 J. Hoinville, A. Bewick, D. Gleeson, R. Jones, O. Kasyutich, E. Mayes, A. Nartowski, B. Warne, J. Wiggins and K. Wong, *J. Appl. Phys.*, 2003, **93**, 7187–7189.

64 H. Ramezani-Dakhel, L. Ruan, Y. Huang and H. Heinz, *Adv. Funct. Mater.*, 2015, **25**, 1374–1384.

65 T. Sakamoto, A. Oichi, Y. Oaki, T. Nishimura, A. Sugawara and T. Kato, *Cryst. Growth Des.*, 2008, **9**, 622–625.

66 L. Ruan, H. Ramezani-Dakhel, C.-Y. Chiu, E. Zhu, Y. Li, H. Heinz and Y. Huang, *Nano Lett.*, 2013, **13**, 840–846.

67 J. Li, N. Menguy, C. Gatel, V. Boureau, E. Snoeck, G. Patriarche, E. Leroy and Y. Pan, *J. R. Soc., Interface*, 2015, **12**, 20141288.

68 C. Jeffryes, S. N. Agathos and G. Rorrer, *Curr. Opin. Biotechnol.*, 2015, **33**, 23–31.

69 M. Matmor and N. Ashkenasy, *J. Mater. Chem.*, 2011, **21**, 968–974.

70 S. M. Luke, B. T. Hallam and P. Vukusic, *Appl. Opt.*, 2010, **49**, 4246.

71 I. Horcas, R. Fernandez, J. M. Gomez-Rodriguez, J. Colchero, J. Gomez-Herrero and A. M. Baro, *Rev. Sci. Instrum.*, 2007, **78**, 13705.

72 Y. Wang, J. E. Panzik, B. Kiefer and K. K. M. Lee, *Sci. Rep.*, 2012, **2**, 520.